IEEE Open Journal of
Power Electronics

Received 10 April 2024; revised 7 May 2024; accepted 8 May 2024. Date of publication 13 May 2024;
date of current version 28 May 2024. The review of this article was arranged by Associate Editor
Xiaoqing Song.

Digital Object Identifier 10.1109/OJPEL.2024.3400291

Mechanical Stress Effects on 4H-Silicon Carbide Power Diodes

TAKAYA SUGIURA (Member, IEEE), KAZUMA YAMASHITA, AND NOBUHIKO NAKANO (Member, IEEE)

Department of Electronics and Electrical Engineering, Keio University, Yokohama 223-8522, Japan

CORRESPONDING AUTHOR: TAKAYA SUGIURA (e-mail: takaya_sugiura@ieee.org)

This work was supported by VLSI Design and Education Center (VDEC), University of Tokyo, in collaboration with Synopsys, Inc.

ABSTRACT This study discusses the effect of stress on 4H-silicon carbide (4H-SiC) power diodes using numerical simulations. Two power diodes were evaluated; namely, a 600 V PiN diode and 1.8 kV junction barrier Schottky **(JBS)** diode. Stress changes the carrier mobilities in the material of the PiN diode of a bipolar diode; that is, the mobility is enhanced by the piezoresistive effect, which minimizes the on-resistance or leakage current. The simulation results demonstrate that compressive stress can have a positive effect on the device operation, particularly in p^+-substrate power diodes. Regarding the JBS diode, the GPa-order tensile stress positively effects both forward and reverse characteristics. A cantilever structure is suitable for JBS diodes, and press-pack packaging for PiN diodes can enhance the device characteristics.

INDEX TERMS 4H-silicon carbide, Junction barrier Schottky diode, mechanical stress, numerical analysis, piezoresistance, PiN diode, power electronics.

I. INTRODUCTION

Wide-bandgap semiconductors are considered as power electronic materials that can potentially replace the conventionally used silicon [1]. Silicon carbide (SiC) is considered a potential candidate for bandgap semiconductors because it provides excellent material properties with a high robustness against voltage, temperature, and chemical corrosion as well as a high Baliga's figure of merit (BFOM) compared to silicon [2], [3]. Its diverse applications include railroads, electric vehicles, and renewable energy [4], [5], [6].

Among the different power devices available, power diodes are considered the simplest, which can be used to regularize signals owing to their high-voltage robustness and high-speed switching frequency. There are two types of power diodes: pn-diode (PiN diodes) and Schottky barrier diodes (SBD). SBDs feature high-speed switching but low-voltage robustness [7]. PiN diodes are suitable for large-power applications; however, 600 - 1,200 V breakdown voltage devices are required for commercial applications.

For power diodes, a low on-resistance and small leakage current are crucial factors that minimize power losses. However, it is difficult to balance both because higher mobility enhances the conductivity of the material, resulting in a small on-resistance and large leakage current. Therefore, the device structure must be optimized to maximize the performance [8]. The device performance can also be improved by enhancing the mobility by applying mechanical stress [9], [10], [11], [12]. The change in mobility due to mechanical stress is known as the piezoresistive effect and is generally used for mechanical stress sensors. Furthermore, strained Si is another approach used to enhance the device performance [13], [14]. Although SiC reportedly induces a significantly smaller mobility change than Si or Ge, it is considered effective in improving the device performance. Research regarding the effects of mechanical stress on 4H-SiC devices remains limited [15], [16], and comprehensive studies are necessary.

This study evaluated the effects of mechanical stress on 4H-SiC PiN power diodes and junction barrier Schottky (JBS) diodes to enhance device performance; 600 V PiN diodes and a 1.8 kV JBS diode were considered.

II. UNDERLYING PHYSICS

A. 4H-SILICON CARBIDE POWER DIODES

SiC materials can be potentially used as next-generation semiconductors in power-electronics applications. Among the SiC

polytypes available, 4H-SiC is considered mainstream (highest BFOM) in the field [2], [3]. The device types are diverse and include pn-diodes (PiN diodes), Schottky barrier diodes (SBDs), thyristors, and transistors. SBDs feature high-speed switching because they are unipolar with an n-type bulk such that the majority carrier is an electron with a high mobility. However, a lower breakdown voltage and larger reverse current are its drawbacks. In addition, SBDs require edge termination to enhance the breakdown characteristics of the contact edge and introduce a concentrated electric field, which causes a hard breakdown [19]. Therefore, the main design interests of SBDs focus on edge termination techniques. To overcome these problems, advanced structures such as JBS diodes (or trenched JBS diodes) have been developed [20] to minimize the leakage current.

PiN diodes feature a higher breakdown voltage than that of SBDs, making PiN diodes suitable for power electronic applications, as high-speed switching is unnecessary. Edge termination in PiN diodes is also necessary to achieve high-voltage robustness, such as in the region of 4.5 kV or higher [21], [22]. To obtain large power regulations, a vertical device structure is widely used in SiC owing to its lower material cost compared to gallium nitride (GaN), which is more costly and features a lateral device structure on a silicon substrate [31]. Furthermore, SiC exhibits a higher thermal conductivity than Si and GaN; therefore, its performance is advantageous in the field of power electronics because it exhibits significant self-heating and thermal dissipation.

B. MOBILITY ENHANCEMENT

Mobility enhancement is caused by the stress applied to the material, which is referred to as the piezoresistive effect and is expressed as follows:

$$\frac{\Delta R}{R_0} = \pi_l \sigma_l + \pi_t \sigma_t. \tag{1}$$

where π and σ are the piezoresistive coefficient and applied stress in the longitudinal (parallel to the current flow) and transverse (normal to the current flow) directions, respectively. π is unique to the materials, and Si and Ge exhibit significantly higher values (absolute values greater than 100×10^{-11} Pa^{-1} in certain orientations) than 4H-SiC [12]. However, 4H-SiC is sufficient for piezoresistive effects [17], [18].

Our previous study [9] established a piezoresistive mobility model based on the experimental results using the following expression:

$$\mu_{Piezo} = \frac{\mu_0}{1 + \pi_l \sigma_l + \pi_t \sigma_t}. \tag{2}$$

The aforementioned expression indicates that the mobility increases when the sign of $\pi\sigma$ is negative, and decreases when the sign is positive.

Fig. 1 shows the carrier mobilities of 4H-SiC under longitudinal stress ($\mu_{Piezo} = \mu_0/(1 + \pi_l \sigma_l)$ from (2)) from 1 to 10 GPa (for both tensile and compressive stresses). The mobilities start to change by more than 100 MPa of stress for both the electrons and holes. As π_{11} of the holes is positive and π_{11} of the electrons is negative, the tensile stress decreases the hole mobility and increases the electron mobility. Under compressive stress, reversed responses of increased hole mobility and decreased electron mobility were observed. A crucial factor is the high sensitivity of the hole mobility under a compressive stress, which is 2.8 times larger at a stress of 10 GPa.

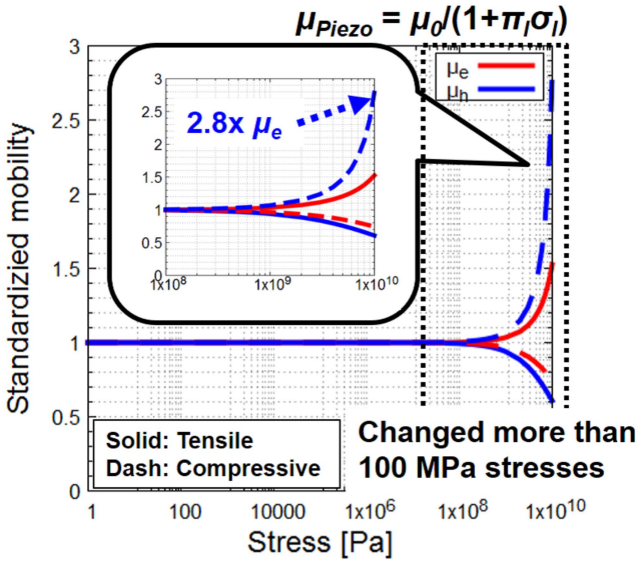

FIGURE 1. Calculated electron and hole mobilities (stabilized) of 4H-SiC under stress from (2).

TABLE 1. Simulation Modeling in This Study

Physics	Value
Material	4H-silicon carbide
Carrier generation rate	1×10^{12} cm^{-3}/s
Carrier mobility	Arora model for 4H-SiC parameters [25], [26]
Saturation velocity	2.2×10^7 cm/s [27]
Carrier lifetime	2.5 μs (electron) 0.5 μs (hole)
Impact ionization	Niwa's model [24]
Dopant activation	Incomplete ionization [28]
Self-heating	Thermodynamic [29] (with generation-recombination heating)
Piezoresistance model	Kanda's model [30]
π_{11}	6.43×10^{-11} Pa^{-1} (p-type) -3.4×10^{-11} Pa^{-1} (n-type) [12]
π_{12}	-5.12×10^{-11} Pa^{-1} (p-type) 6.15×10^{-11} Pa^{-1} (n-type) [12]

III. SIMULATION MODELING

The Sentaurus Technology Computer-Aided-Design (TCAD) software provided by Synopsys, Inc. was used [26]. The fundamental simulation modeling parameters used in this study are listed in Table 1. For the piezoresistance model, we used Kanda's piezoresistance mobility model [30], which utilizes the $< 0001 >$ orientation and enables the substitution

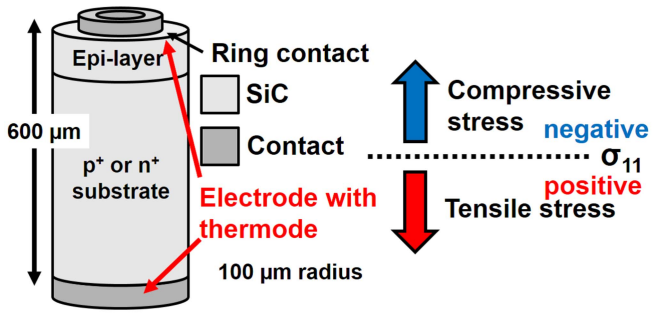

FIGURE 2. Illustration of 4H-SiC PiN diode modeling.

TABLE 2. Device Characteristics of PiN Diodes Modeled in This Study [24]

Region	p^+-substrate	n^+-substrate
Top	1×10^{19} cm^{-3} n-type 1 μm	1×10^{19} cm^{-3} p-type 1 μm
Multiplication	4.0×10^{16} cm^{-3} n-type 13 μm	3.7×10^{16} cm^{-3} p-type 12 μm
Substrate	2.0×10^{18} cm^{-3} p-type	2.0×10^{18} cm^{-3} n-type

of hexagonal crystals. The parameters listed in Table 1 are common for the PiN and JBS diodes; detailed structural and additional modeling parameters are listed in the following sections.

IV. PIN DIODES

For simulation modeling, experiments regarding the 4H-SiC power diode breakdowns at different temperatures are described in [24]. Furthermore, two diodes doped with different substrates and having similar breakdown voltages of approximately 600 V were used in the modeling. The device structure is illustrated in Fig. 2. The two diodes were non-punch-through (NPT). The device characteristics are listed in Table 2. The top and multiplication layers are the epi-layers; therefore, thicknesses of 13–14 μm are ensured. For simpler modeling, we adopted cylindrical device structures instead of mesa structures. A difference in the breakdown voltages was observed owing to the concentrated electric field. Additionally, a two-dimensional (2D)-grid with a cylindrical boundary condition was introduced to simplify the modeling process.

Before the evaluation, we verified the simulation model by reproducing the reverse-biased breakdown phenomenon. Fig. 3 shows the reverse-biased breakdown simulations of the 4H-SiC power diodes. An experiment was conducted to determine the impact ionization coefficients of 4H-SiC based on the avalanche breakdown phenomenon of the photodiodes. The contact structures were in the form of rings. The breakdown characteristics obtained for both the p^+- and n^+-substrates sufficiently matched, with similar breakdown voltages of 600 V, even for the cylindrical structures. The R_{on} value for each diode was 12.4 mΩ-cm^2 and 6.7 mΩ-cm^2 for the p^+ and n^+ substrates, respectively. The effects of both

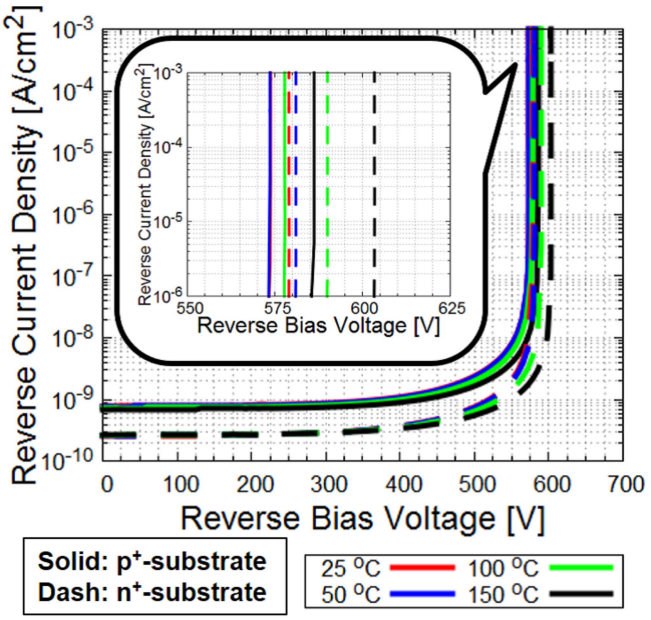

FIGURE 3. Reversed J–V characteristics of PiN diodes for modeling verification.

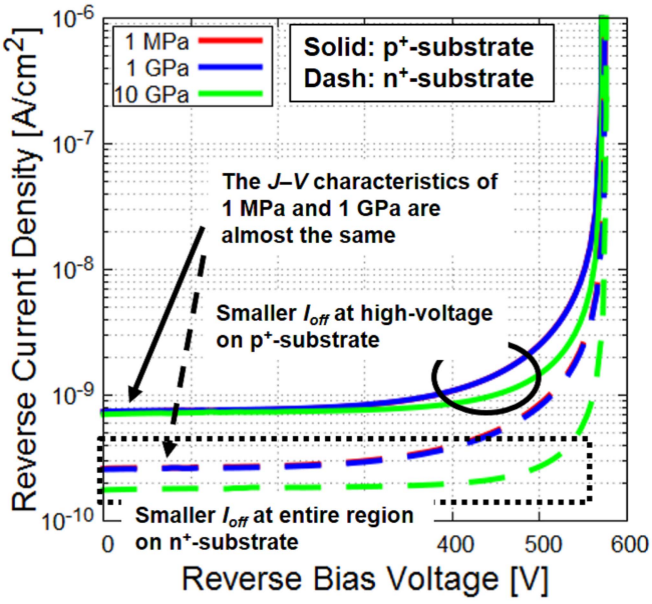

FIGURE 4. Reversed J–V characteristics of PiN diodes under the tensile stress.

the tensile and compressive stresses under DC conditions are discussed.

Tensile stress suppresses the hole mobility and enhances the electron mobility via the longitudinal piezoresistive coefficients. Fig. 4 shows the reversed J–V characteristics under tensile stresses of up to 10 GPa. Smaller leakage currents, especially of the n^+-substrate, can be observed. Although the n^+-substrate is affected by the increased electron mobility, its leakage current is suppressed, which is likely owing to the top p^+-doping layer. The breakdown voltages were unaffected by

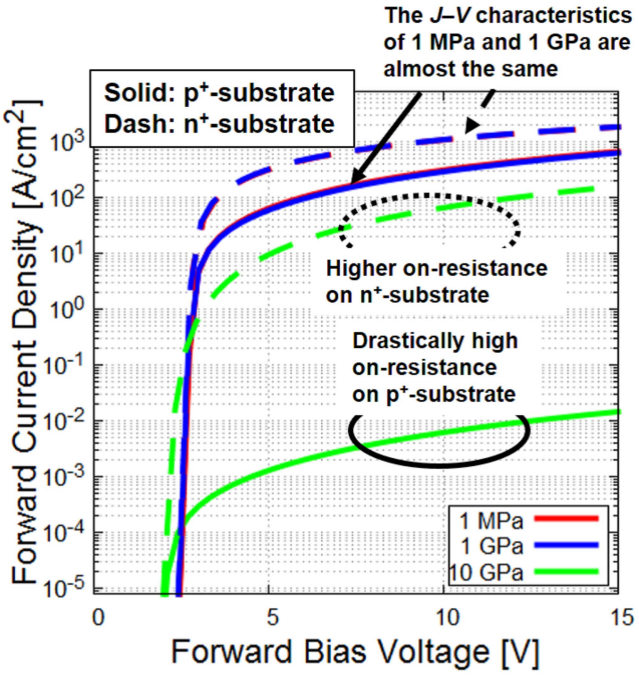

FIGURE 5. Forward J–V characteristics of PiN diodes under the tensile stress.

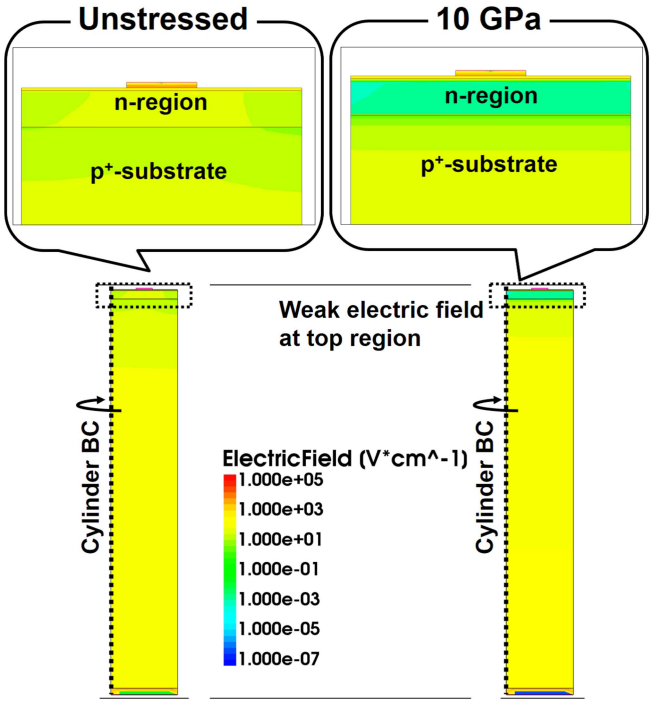

FIGURE 6. Electric field distributions of unstressed and 10 GPa-stressed conditions at a 10 V forward bias.

the increase in mobility. However, regarding the forward J–V characteristics shown in Fig. 5, both power diodes exhibited significantly increased on-resistances, particularly for the p^+-substrate.

Fig. 6 shows the electric field distributions of the p^+-substrate diodes under unstressed and 10 GPa-stressed conditions at a forward-biased voltage of 10 V. The higher on-resistance can be attributed to the weak electric field that appears in the top region of the diodes under high-stress conditions. Because the electric field strength corresponds to the carrier transport volume, a weak electric field increases the on-resistance. Changes in the carrier mobilities in both the p- and n-regions in different orientations (an increase in electrons and a decrease in holes) caused the electric field to change. As the electron has a significantly larger mobility than that of the hole, the mobility change resulted in decreased carrier volumes. The electrons escaped rapidly from the device; however, the holes were significantly slower than the electrons, thus supplying holes requires time. Regardless of the type of substrate doping used, tensile stress has a negative effect on the forward-biased conditions. Therefore, the increased majority-carrier mobility gaps between the n-(increased) and p-regions (decreased) result in this phenomenon. The increased majority-carrier mobility gaps at the junction inhibit the carrier transport, resulting in an increase in the on-resistance.

Compressive stress enhances the hole mobility and suppresses electron mobility via the longitudinal piezoresistive coefficients. Fig. 7 shows the reverse J–V characteristics under compressive stresses of up to 10 GPa. In contrast to the tensile stress conditions, the leakage currents exhibited

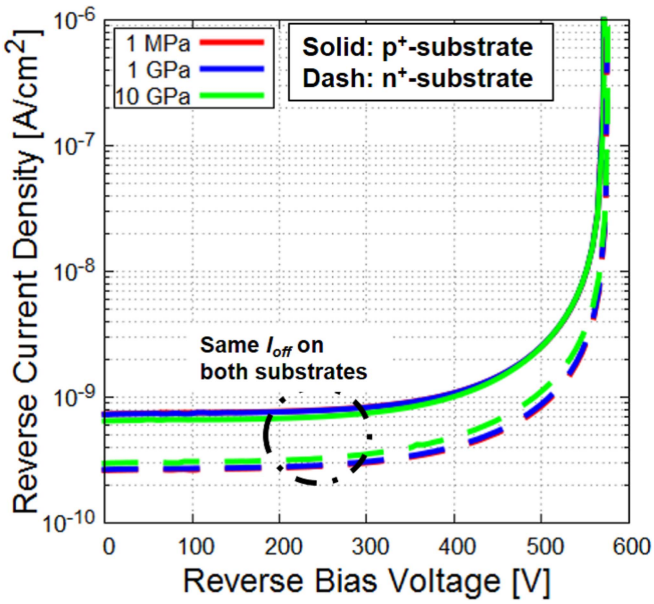

FIGURE 7. Reverse J–V characteristics of PiN diodes under the compressive stress.

negligible changes owing to the stresses, and the breakdown voltages were the same. Fig. 8 shows the forward-biased J–V characteristics under the same conditions. In particular, an enhanced on-resistance was confirmed for the p^+-substrate, which is better for power diodes. The n^+ substrate demonstrated a smaller benefit; however, a higher current was

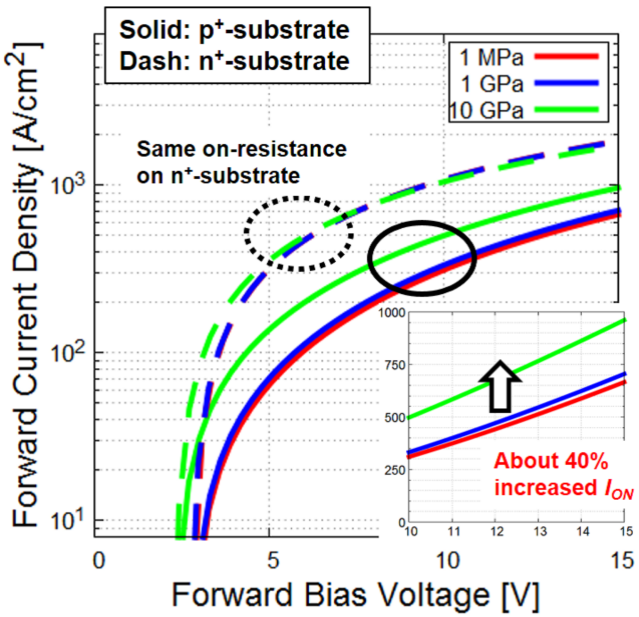

FIGURE 8. Forward J–V characteristics of PiN diodes under a compressive stress.

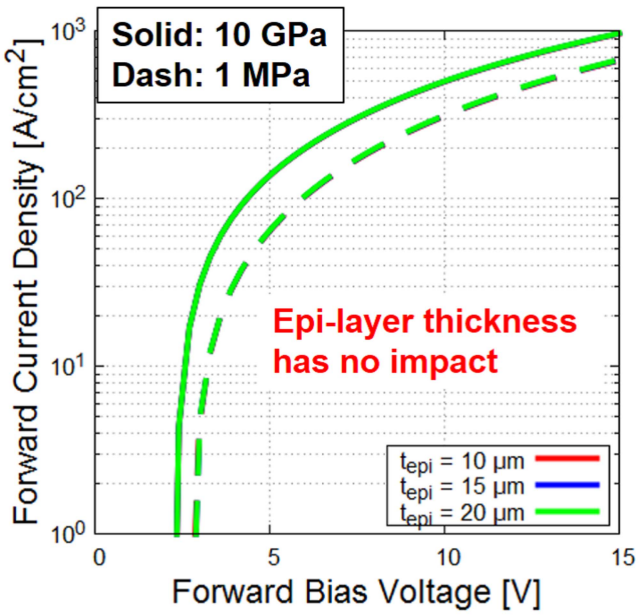

FIGURE 9. Effect of the epi-layer thickness on the p+-substrate of a PiN diode at the forward J–V characteristics.

obtained at a smaller bias voltage, which is better for switching. The reverse phenomenon from the tensile stress condition enhanced the carrier transport at the junction of both substrates. Fig. 9 shows the evaluation of the effect of the epi-layer thickness on the p^+-substrate during the forward-biased operation. The results indicate that the thickness had no impact on the device operation; the same on-current enhancement was observed regardless of the thickness.

TABLE 3. Stress Effects on the Performance of PiN Diodes

Performance	Tensile	Compressive
Breakdown voltage	No differences	No differences
Leak current	Decreased (for both substrates)	No differences
On-resistance	Increased	Minimized (for p^+-substrate)

TABLE 4. Simulation Modeling of the Junction-Barrier Schottky Diode in This Study [20]

Physics	Value
Material	4H-silicon carbide
Thickness	350 μm
Epi-layer doping concentration	8×10^{15} cm^{-3}
Epi-layer thickness	12 μm
Substrate doping concentration	5×10^{19} cm^{-3} [36]
Junction spacing	0.6 μm
Nickel's work function	5.2 eV [37]

Table 3 summarizes the effects of stress on the performance. A positive effect on the on-resistance was observed for the p^+-substrate when a compressive stress was applied. The aforementioned discussion indicates that compressive stress benefits the diode operation. The magnitude of the stress at 10 GPa was large; however, it is expected to be sufficient within the yield stress [32]. This significantly enhanced mobility contributed to an increased I_{ON}, as shown in Fig. 8.

In this study, the effects of mechanical stress on bipolar SiC devices were evaluated based on reports regarding unipolar SiC MOSFET devices [33], [15]. The p^+-substrate 4H-SiC power diodes were recently developed [34]; therefore, their applications are expected. In addition, when a large tensile stress is applied, the device performance is weakened, particularly for p^+-substrate devices.

V. JUNCTION BARRIER SCHOTTKY DIODES

This section discusses the JBS diode characteristics. An example of a 4H-SiC JBS diode designed using numerical simulations is based on [20]. The modeling parameters used for the study of the JBS diode are listed in Table 4. The 4H-SiC/nickel (virtual) interface was set as a Schottky contact with a nickel work function of 5.2 eV [36]. This model enables the Schottky interface of n-drift/nickel only, and the p^+-implantation/nickel interface is ohmic. Fig. 10 shows the simulation model of the JBS diode used in this study; a) simulation grid, b) forward J–V characteristic, and c) reverse J–V characteristics. The graph shows that the device features a breakdown voltage of 1.8 kV, which sufficiently matches with the reference. The on-resistance of the simulation resulted in 6.94 mΩ-cm^2 with a V_{th} of 0.9 V. Here, the difference from the literature regarding the simulated one in the on-resistance is likely owing to the different mobility models: the Arora mobility model for 4H-SiC in the present study and the Caughey–Thomas model, which was originally developed for silicon [38] in [20]. The differences between our model and the experiments presented in [20] are owing to the device

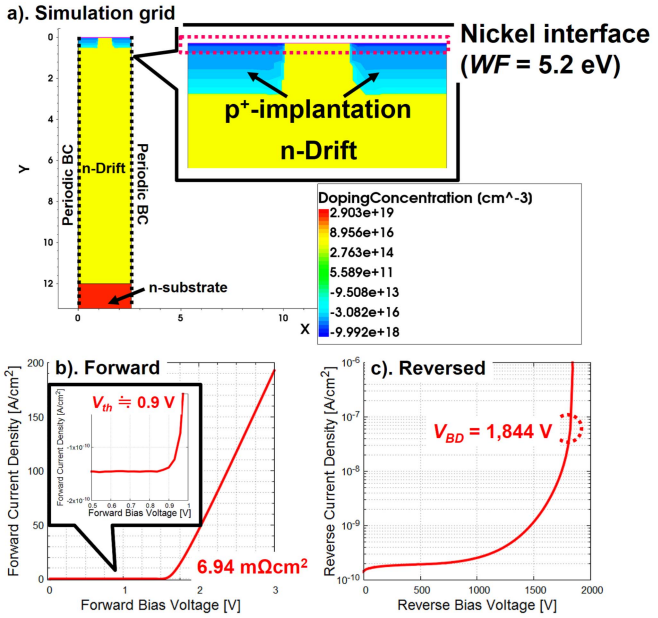

FIGURE 10. Simulation modeling of the JBS diode: (a) Simulation grid, (b) forward J–V characteristic, and (c) reverse J–V characteristic.

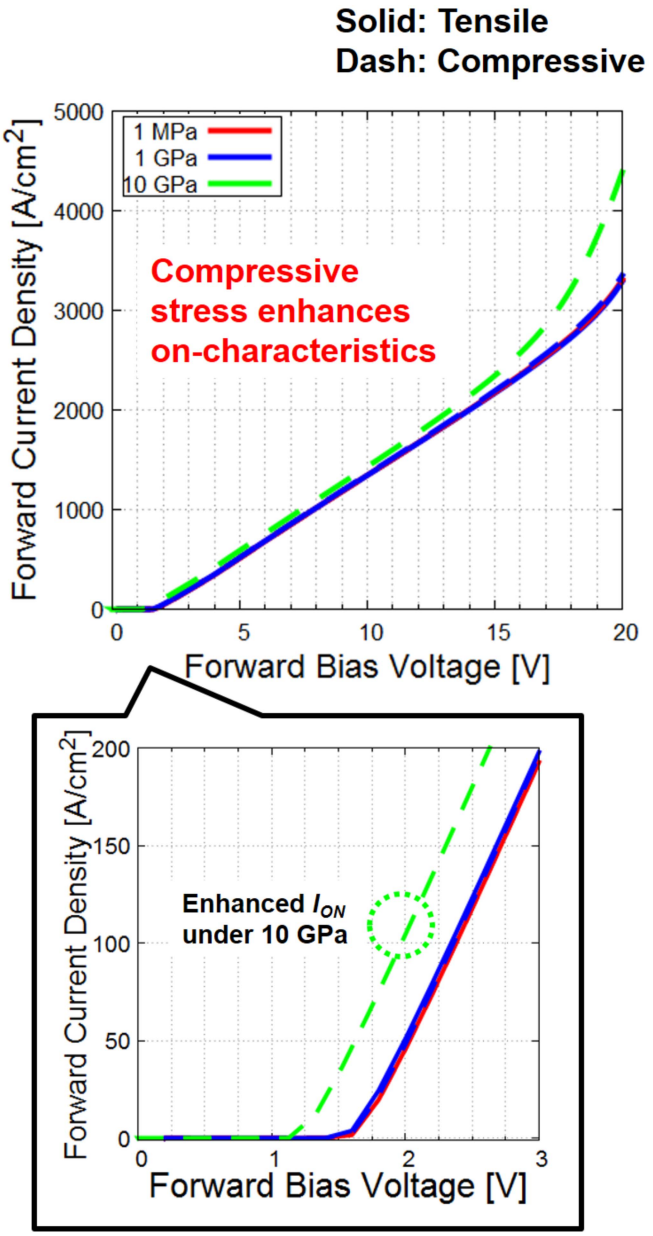

FIGURE 11. Forward J–V characteristics of JBS diode under mechanical stress.

structure; our model only treats the JBS interface; however, the realistic device was significantly larger in size and included a field-limiting ring (FLR) [37]. These differences are critical for the breakdown voltage because the FLR effect is neglected; a similar difference was also observed in [20]. For the forward operation, our model sufficiently reproduced the J–V characteristics when the junction spacing was 0.6 μm.

Mechanical stresses of 1 MPa, 1 GPa, and 10 GPa under tensile and compressive conditions were considered for the following. Here, a tensile stress of 10 GPa complicates the convergence problem, resulting in unintentional device operations; therefore, the result of this condition was removed. Fig. 11 illustrates the forward J–V characteristics under mechanical stress. The compressive stress enhanced the on-characteristics, to which the GPa-order mechanical stress contributed. This effect increases when a voltage of higher than 15 V is applied, and will be useful for designing low-loss power devices. This compressive stress also works as the negative for reverse operations, as shown in Fig. 12. When a compressive stress of 10 GPa was applied, the breakdown voltage decreased from being higher than 1,800 V to nearly 1.600 V, resulting in a decrease of more than 200 V. A higher breakdown voltage was maintained; this phenomenon was negligible when the devices were used at a mid-range voltage. For a tensile strength of 10 GPa, although the data are not included in the graph, the characteristics of 1 MPa and 1 GPa demonstrated slightly increased breakdown voltages; therefore, this stress is expected to provide a significantly higher breakdown voltage.

Fig. 13 shows the GPa-order tensile stress effects on both the forward (graph a).) and reverse (graph b).) J–V characteristics. Regarding the forward characteristics, enhanced on-characteristics were observed when the mechanical stress exceeded 5 GPa. As shown in Fig. 1, a GPa tensile stress results in an enhanced electron mobility, resulting in an improved performance. For the reverse characteristics, the tensile stress also increased the breakdown voltage (although the improvements were small). Here, improved on-characteristics were also observed in the compressive stress, as shown in Fig. 11, because the JBS diode includes both the n-regions (n^--drift and n^+-substrate) and p-region (p^+-implantation). Therefore, the compressive stress improved the p-region, and both tensile and compressive stresses were beneficial for the JBS diode.

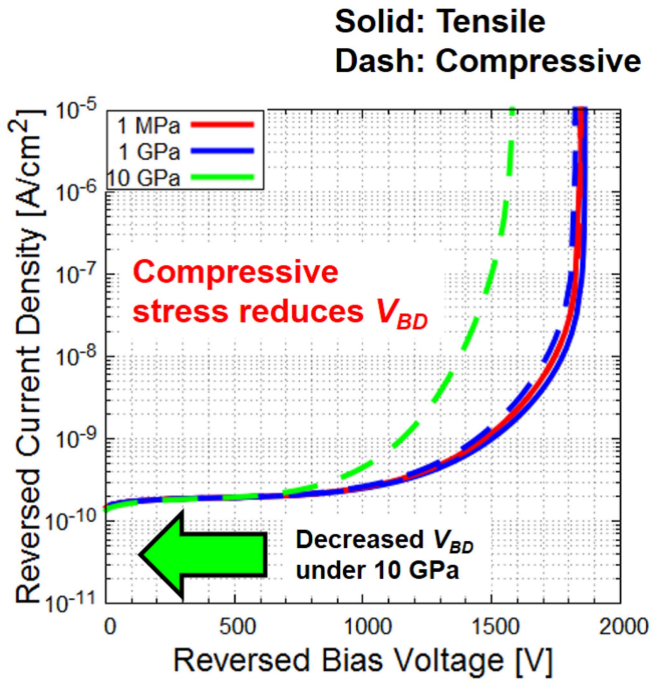

FIGURE 12. Reverse J–V characteristics of JBS diode under mechanical stress.

Compared with the PiN diodes, the main difference of the JBS diode is the breakdown voltage response. The breakdown voltage of the JBS diode varied when a large stress was applied; however, the PiN diode demonstrated no changes with the stress. This may be owing to the device structure; namely, the PiN diode of the bipolar device and JBS diode of the unipolar device. The main reason for the decreased breakdown voltage is the increased mobility, and the unipolar structure directly reflects its effect on the device performance. For the bipolar structures of the PiN diodes, the reverse responses of n-SiC and p-SiC eliminate the variation in the breakdown voltage, as the mechanical stress increases the mobility of SiC on one side and decreases it on the other. For forward operations, both the tensile and compressive stresses were effective in improving the device operation, which is an advantage over the PiN diode. To enhance the device performance, GPa-order mechanical stress is necessary; this large tensile stress results in both improved forward and reverse operations.

Table 5 summarizes the performance of the JBS diode under various stress conditions. However, as the tensile stress worked better for both the forward and reverse operations, as shown in Fig. 11, a smaller stress of less than GPa featured a slightly increased on-resistance (although it was nearly negligible). The MPa- and GPa-order tensile stresses apparently make the p- (effect of decreased μ_h) and n- (effect of improved μ_e) regions dominant, respectively. Regardless, a GPa-level stress is necessary to change the device characteristics.

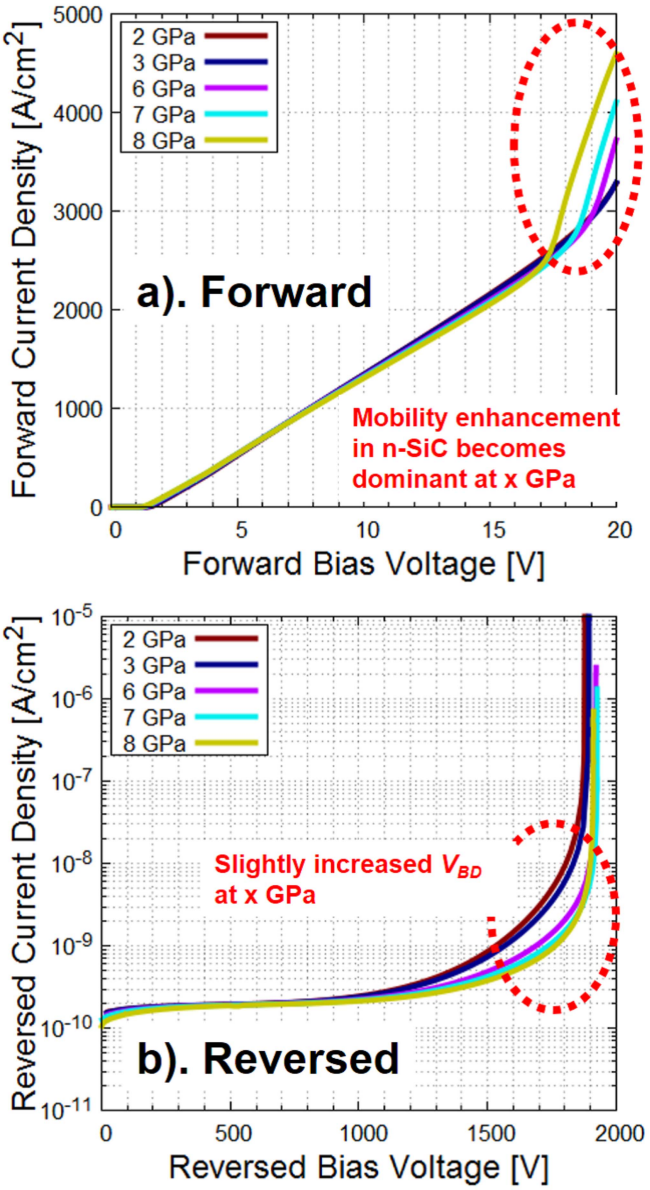

FIGURE 13. (a) Forward and (b) reverse J–V characteristics of the JBS diode under a GPa-order tensile mechanical stress.

TABLE 5. Stress Effects on the Performance of the JBS Diode

Performance	Tensile	Compressive
Breakdown voltage	Increased	Decreased
Leak current	No difference	No difference
On-resistance	Minimized (under GPa)	Minimized
Solution	Cantilever	Press-pack packaging

VI. SUMMARY

The results demonstrated that a large mechanical stress at the GPa scale is mandatory to change the device characteristics. For the JBS diode, the GPa-scale tensile stress was advantageous for both the forward and reverse characteristics. Therefore, applying an aggressive level of stress is better, such as by utilizing cantilever structures that are used for

piezoresistive sensors [12]. In addition, compressive stress only improved forward operations, particularly in the low-voltage region, and certain situations may be more suitable for applying a compressive stress rather than a tensile stress. For PiN diodes, a certain amount of compressive stress desirably increased the on-current; therefore, utilizing mechanical stress will improve the performance. When low-loss power devices are designed, tensile stress is good for the JBS diode, whereas the compressive stress is good for the PiN diodes. Because GPa-scale stress is large and difficult to obtain from natural mechanical properties, the intended stress can be obtained by press-pack packaging for compressive stress applications [39]. This technique is widely used in power electronics to achieve a pressure contact while avoiding wire bonding and soldering. The findings of this study contribute to the application of this technique. Press-pack packaging is generally used for high-voltage power devices [40]. Our results demonstrated that the entire voltage range for PiN diodes and higher than mid-range ($>$15 V) for the JBS diode provides the mechanical stress.

VII. CONCLUSION

The effects of stress on 4H-SiC power diodes were evaluated. For the PiN bipolar diodes, tensile stress has an adverse effect on the on-resistances owing to the increased majority-carrier mobility gaps between the p- and n-regions, which inhibit carrier transport, whereas compressive stress benefits device operations by the opposite effect, particularly at the p^+-substrate. The breakdown voltages were found to be independent of the mechanical stress. For the JBS unipolar diode, both the on-resistance and breakdown voltage varied with the mechanical stress. Applying a tensile stress at the GPa scale demonstrated the potential to improve both the forward and reverse characteristics; therefore, installing the device on the cantilever structure will sufficiently improve the performance. Compressive stress enhanced the on-characteristics; however, it decreased the breakdown voltages. To design low-loss power devices, a large tensile stress is good for JBS diodes, and compressive stress is suitable for PiN diodes. Therefore, the cantilever for the JBS diode and press-pack packaging technique for PiN diodes can be used to obtain the required stress.

REFERENCES

[1] J. Millán, P. Godignon, X. Perpiñà, A. Pérez-Tomás, and J. Rebollo, "A survey of wide bandgap power semiconductor devices," *IEEE Trans. Power Electron.*, vol. 29, no. 5, pp. 2155–2163, May 2014, doi: 10.1109/TPEL.2013.2268900.

[2] A. Q. Huang, "New unipolar switching power device figures of merit," *IEEE Electron Device Lett.*, vol. 25, no. 5, pp. 298–301, May 2004, doi: 10.1109/LED.2004.826533.

[3] F. Li et al., "Status and prospects of cubic silicon carbide power electronics device technology," *Materials*, vol. 14, 2021, Art. no. 5831, doi: 10.3390/ma14195831.

[4] X. She, A. Q. Huang, Ó. Lucia, and B. Ozpineci, "Review of silicon carbide power devices and their applications," *IEEE Trans. Ind. Electron.*, vol. 64, no. 10, pp. 8193–8205, Oct. 2017, doi: 10.1109/TIE.2017.2652401.

[5] T. Kimoto, "Material science and device physics in SiC technology for high-voltage power devices," *Japanese J. Appl. Phys.*, vol. 54, 2015, Art. no. 040103, doi: 10.7567/JJAP.54.040103.

[6] E. Papanasam, B. K. Prashanth, B. Chanthini, E. Manikandan, and L. Agarwal, "A comprehensive review of recent progress, prospect and challenges of silicon carbide and its applications," *Silicon*, vol. 14, pp. 12887–12900, 2022, doi: 10.1007/s12633-022-01998-9.

[7] T. Kimoto, "High-voltage SiC power devices for improved energy efficiency," *Proc. Jpn. Acad., Ser. B*, vol. 98, pp. 161–189, 2022, doi: 10.2183/pjab.98.011.

[8] K. Nomura, T. Kondoh, T. Ishikawa, S. Yamasaki, K. Yaji, and K. Fujita, "Doping profile optimization for power devices using topology optimization," *IEEE Trans. Electron Devices*, vol. 65, no. 9, pp. 3869–3877, Sep. 2018, doi: 10.1109/TED.2018.2854637.

[9] T. Sugiura, N. Takahashi, and N. Nakano, "The piezoresistive mobility modeling for cubic and hexagonal silicon carbide crystals," *J. Appl. Phys.*, vol. 127, 2020, Art. no. 245113, doi: 10.1063/5.0006830.

[10] T. Sugiura, N. Takahashi, R. Sakota, K. Matsuda, and N. Nakano, "High-temperature piezoresistance of silicon carbide and gallium nitride materials," *IEEE J. Electron Devices Soc.*, vol. 10, pp. 203–211, 2022, doi: 10.1109/JEDS.2022.3150915.

[11] T. Sugiura, N. Takahashi, R. Sakota, K. Matsuda, and N Nakano, "Piezoresistive thermal characteristics of aluminum-doped p-type 3C-silicon carbides," *IEEE J. Electron Devices Soc.*, vol. 10, pp. 547–553, 2022, doi: 10.1109/JEDS.2022.3191543.

[12] T. Sugiura, K. Matsuda, and N. Nakano, "Review: Numerical simulations of semiconductor piezoresistance for computer-aided designs," *IEEE J. Electron Devices Soc.*, vol. 11, pp. 325–336, 2023, doi: 10.1109/JEDS.2023.3281866.

[13] K. Uchida et al., "Experimental study of biaxial and uniaxial strain effects on carrier mobility in bulk and ultrathin-body SOI MOSFETs," in *Proc. IEEE IEDM Tech. Dig. Int. Electron Devices Meeting*, 2004, pp. 229–232, doi: 10.1109/IEDM.2004.1419116.

[14] T. Krishnamohan, Z. Krivokapic, K. Uchida, Y. Nishi, and K. C. Saraswat, "High-mobility ultrathin strained Ge MOSFETs on bulk and SOI with low band-to-band tunnelling leakage: Experiments," *IEEE Trans. Electron Devices*, vol. 53, no. 5, pp. 990–999, May 2006, doi: 10.1109/TED.2006.872362.

[15] M. Kato, A. Goryu, A. Kano, K. Takao, K. Hirohata, and S. Izumi, "Evaluation method for performance of SiC power module by electro-thermal-anisotropic stress coupled analysis," in *Proc. ASME Int. Mech. Engineer. Congr. Expo.*, 2019, Paper V010T13A001,doi: 10.1115/IMECE2018-86626.

[16] W. Wu, S. Liu, J. Zhu, and W. Sun, "Comprehensive investigation on mechanical strain-induced performance boosts in LDMOS," in *Proc. IEEE 30th Int. Symp. Power Semicond. Devices ICs*, 2018, pp. 60–63, doi: 10.1109/ISPSD.2018.8393602.

[17] T. Nguyen et al., "Isotropic piezoresistance of p-type 4H-SiC in the (0001) plane," *Appl. Phys. Lett.*, vol. 113, 2018, Art. no. 012104, doi: 10.1063/1.5037545.

[18] B. Tian, H. Shang, D. Wang, Y. Liu, and W. Wang, "Investigation on piezoresistive effect of n-type 4H-SiC based on all-SiC pressure sensors," *IEEE Sensors J.*, vol. 22, no. 7, pp. 6435–6441, Apr. 2022, doi: 10.1109/JSEN.2022.3153630.

[19] M. Zhang, B. Li, M. Hua, and J. Wei, "Investigation of electrical contacts to P-grid in SiC power devices based on charge storage effect and dynamic degradation," *Electronics*, vol. 9, 2020, Art. no. 1723, doi: 10.3390/electronics9101723.

[20] N. Ren, J. Wang, and K. Sheng, "Design and experimental study of 4H-SiC trenched junction barrier Schottky diodes," *IEEE Trans. Electron Devices*, vol. 61, no. 7, pp. 2459–2465, Jul. 2014, doi: 10.1109/TED.2014.2320979.

[21] W. Sung and B. J. Baliga, "A near ideal edge termination technique for 4500V 4H-SiC devices: The hybrid junction termination extension," *IEEE Electron Devices Lett.*, vol. 37, no. 12, pp. 1609–1612, Dec. 2016, doi: 10.1109/LED.2016.2623423.

[22] J. Li et al., "High-voltage 4H-SiC PiN diodes with the etched implant junction termination extension," *J. Semicond.*, vol. 38, 2017, Art. no. 024003, doi: 10.1088/1674-4926/38/2/024003.

[23] N. Iwamuro, "4 - SiC power device design and fabrication," in *Proc. Wide Bandgap Semicon. Power Devices Mater. Phys. Des. Appl.*, 2019, pp. 79–149, doi: 10.1016/B978-0-08-102306-8.00004-6.

[24] H. Niwa, J. Suda, and T. Kimoto, "Impact ionization coefficients in 4H-SiC towards ultrahigh-voltage power devices," *IEEE*

Trans. Electron Devices, vol. 62, no. 10, pp. 3326–3333, Oct. 2015, doi: 10.1109/TED.2015.2466445.

[25] N. D. Arora, J. R. Hauser, and D. J. Roulston, "Electron and hole mobilities in silicon as a function of concentration and temperature," *IEEE Trans. Electron Devices*, vol. EV-29, no. 2, pp. 292–295, Feb. 1982, doi: 10.1109/T-ED.1982.20698.

[26] Sentaurus Synopsys TCAD, "Software Release S-2021-06-SP1," Sentaurus Device, Mountain View, CA, USA, Tech. Rep. S-2021.06-SP1, 2021.

[27] I. A. Khan and J. A. Cooper, "Measurement of high-field electron transport in silicon carbide," *IEEE Trans. Electron Devices*, vol. 47, no. 2, pp. 269–273, Feb. 2000, doi: 10.1109/16.822266.

[28] M. Lades, W. Kaindl, N. Kaminski, E. Niemann, and G. Wachutka, "Dynamics of incomplete ionized dopants and their impact on 4H/6H-SiC devices," *IEEE Trans. Electron Devices*, vol. 46, no. 3, pp. 598–604, Mar. 1999, doi: 10.1109/16.748884.

[29] G. Wachutka, "An extended thermodynamic model for the simultaneous simulation of the thermal and electrical behaviour of semiconductor devices," in *Proc. 6th Int. Conf. Numer. Anal. Semicond. Device Integr. Circuits*, 1989, pp. 409–414.

[30] K. Matsuda, K. Suzuki, K. Yamamura, and Y. Kanda, "Nonlinear piezoresistance effects in silicon," *J. Appl. Phys.*, vol. 73, no. 4, pp. 1838–1847, Feb. 1993, doi: 10.1063/1.353169.

[31] N. Kaminski and O. Hilt, "SiC and GaN devices - wide bandgap is not all the same," *IET Circuits Devices Syst.*, vol. 8, pp. 227–236, 2014, doi: 10.1049/iet-cds.2013.0223.

[32] V. I. Ivaschenko, P. E. A. Turchi, and V. I. Shevchenko, "Simulations of the mechanical properties of crystalline, nanocrystalline, and amorphous SiC and Si," *Phys. Rev. B.*, vol. 75, 2007, Art. no. 085209, doi: 10.1103/PhysRevB.75.085209.

[33] A. Goryu, M. Kato, A. Kano, S. Izumi, and K. Hirohata, "Evaluation method for mechanical stress dependence of the electrical characteristics of SiC MOSFET for electro-thermal-structural coupled analysis," in *Proc. ASME Int. Mech. Eng. Congr. Expo.*, 2017, Paper V010T13A019, doi: 10.1115/IMECE2017-72027.

[34] A. Koyama et al., "Low V_F 4H-SiC N-i-P diodes using newly developed low-resistivity p-type substrates," *Japanese J. Appl. Phys.*, vol. 59, 2020, Art. no. SGGD14, doi: 10.35848/1347-4065/ab6b7d.

[35] A. F. d. Silva, J. Peot, S. Contreras, B. E. Sernelius, C. Persson, and J. Camassel, "Electrical resistivity and metal-nonmetal transition in n-type doped 4H-SiC," *Phys. Rev. B.*, vol. 74, 2006, Art. no. 245201, doi: 10.1103/PhysRevB.74.245201.

[36] B. G. Baker, B. B. Johnson, and G. L. C. Maire, "Photoelectric work function measurements on nickel crystals and films," *Surf. Sci.*, vol. 24, no. 2, pp. 572–586, Feb. 1971, doi: 10.1016/0039-6028(71)90282-2.

[37] J. Zhang, H. Luo, H. Wu, Z. Wang, B. Zheng, and X. Chen, "Design and optimization of cell and field limiting ring termination for 1200 V 4H-SiC Junction Barrier Schottky (JBS) diode," in *Proc. IEEE 23rd Int. Conf. Electron. Packag. Technol.*, 2022, pp. 1–5, doi: 10.1109/ICEPT56209.2022.9873379.

[38] D. M. Caughey and R. E. Thomas, "Carrier mobilities in silicon empirically related to doping and field," *Proc. IEEE*, vol. 55, no. 12, pp. 2192–2193, Dec. 1967, doi: 10.1109/PROC.1967.6123.

[39] N. Zhu, H. A. Mantooth, D. Xu, M. Chen, and M. D. Glover, "A solution to press-pack packaging of SiC MOSFETs," *IEEE Trans. Ind. Electron.*, vol. 64, no. 10, pp. 8224–8234, Oct. 2017, doi: 10.1109/TIE.2017.2686365.

[40] L. Han, L. Liang, Y. Wang, X. Tang, and S. Bai, "Performance limits of high voltage press-pack SiC IGBT and SiC MOSFET devices," *Power Electron. Devices Comp.*, vol. 3, 2022, Art. no. 100019, doi: 10.1016/j.pedc.2022.100019.